An Indoor Visible Light Positioning System Using Tilted LEDs with High Accuracy

Neha Chaudhary, Othman Isam Younus, Luis Nero Alves, Zabih Ghassemlooy, Stanislav Zvanovec, Hoa Le-Minh

sensors

MDPI

Article

An Indoor Visible Light Positioning System Using Tilted LEDs with High Accuracy

Neha Chaudhary [1,*], Othman Isam Younus [2], Luis Nero Alves [1], Zabih Ghassemlooy [2], Stanislav Zvanovec [3] and Hoa Le-Minh [2]

[1] Instituto de Telecomunicações and Departamento de Electrónica, Telecomunicações e Informática, Universidade de Aveiro, 3810-193 Aveiro, Portugal; nero@ua.pt
[2] Optical Communications Research Group, Faculty of Engineering and Environment, Northumbria University, Newcastle upon Tyne NE1 8ST, UK; othman.younus@northumbria.ac.uk (O.I.Y.); z.ghassemlooy@northumbria.ac.uk (Z.G.); hoa.le-minh@northumbria.ac.uk (H.L.-M.)
[3] Department of Electromagnetic Field, Faculty of Electrical Engineering, Czech Technical University in Prague, 16627 Prague, Czech Republic; xzvanove@fel.cvut.cz
* Correspondence: neha.chaudhary@ua.pt

Abstract: The accuracy of the received signal strength-based visible light positioning (VLP) system in indoor applications is constrained by the tilt angles of transmitters (Txs) and receivers as well as multipath reflections. In this paper, for the first time, we show that tilting the Tx can be beneficial in VLP systems considering both line of sight (LoS) and non-line of sight transmission paths. With the Txs oriented towards the center of the receiving plane (i.e., the pointing center F), the received power level is maximized due to the LoS components on F. We also show that the proposed scheme offers a significant accuracy improvement of up to ~66% compared with a typical non-tilted Tx VLP at a dedicated location within a room using a low complex linear least square algorithm with polynomial regression. The effect of tilting the Tx on the lighting uniformity is also investigated and results proved that the uniformity achieved complies with the European Standard EN 12464-1. Furthermore, we show that the accuracy of VLP can be further enhanced with a minimum positioning error of 8 mm by changing the height of F.

Keywords: localization; visible light communication; visible light positioning; received signal strength; linear least square; polynomial regression; Tx's tilting

Citation: Chaudhary, N.; Younus, O.I.; Alves, L.N.; Ghassemlooy, Z.; Zvanovec, S.; Le-Minh, H. An Indoor Visible Light Positioning System Using Tilted LEDs with High Accuracy. *Sensors* **2021**, *21*, 920. https://doi.org/10.3390/s21030920

Academic Editor: Antonio Moschitta
Received: 10 December 2020
Accepted: 26 January 2021
Published: 29 January 2021

1. Introduction

Coronavirus disease 2019 (COVID-19) has had a major impact on society at a global level, where social distancing, monitoring, and tracking has become effective in controlling and reducing the spread of the virus [1]. Precise localization and tracking technologies for use in indoor and outdoor environments will play a crucial role in dealing with COVID-19 and other pandemic outbreaks in the future. Nowadays, indoor positioning has a prominent contribution in day-to-day activities in organizations such as health care centers, airports, shopping malls, manufacturing, underground locations, etc., for the safe operating environments. In indoor environments, both radio frequency (RF) and optical wireless-based technologies could be adopted for localization [2,3]. Although the RF-based global positioning system offers higher penetration rates with reduced accuracy (i.e., in the range of a few meters), it does not work well in indoor environments (and not at all in certain cases such as tunnels, mines, etc.) due to the very weak signal and no direct access to the satellites [4–6]. On the other hand, the light-based system known as a visible light positioning (VLP) system, which uses the light-emitting diodes (LEDs)-based lighting infrastructure, could be used at low cost and high accuracy compared with the RF-based system [7,8].

VLP can be implemented using different techniques. Proximity and scene analysis (i.e., fingerprinting) are considered the simplest methods with relatively low positioning errors ε_p i.e., typically in a range of 10 to 45 cm, depending on the fingerprint database [8–10]. In the scene analysis technique, the estimation process of the relative position can be obtained by comparing the measured value with a pre-measured location of each position and then matching it to determine the real position. However, the measurement can be affected by the distributions of base stations, i.e., transmitters (Txs), shadowing and blocking, as well as the absolute location (i.e., probabilistic and correlation) dependency on pattern recognition techniques [9]. A VLP using two photodiodes (PDs) and an image sensor (IS) was proposed in [7,8,11]. Note, visible light communication (VLC) with IS (composed of a large PD array) naturally fits well with multiple inputs multiple-output systems in indoor and outdoor applications. In IS-based VLP, image-processing techniques can be used to determine the position but at the cost of increased complexity [12]. Note that, in VLP the transmission speeds (i.e., data rates) of the PD and IS are not critical at all since the aim is to achieve positioning with high accuracy [13]. Most research reported on VLP has focused on the investigation of geometrical properties using triangulation/trilateration, fingerprinting, or proximity methods to determine the transmission distance based on establishing a one-to-one relationship between the target location and its received signal strength (RSS). In such works, the analyses were based on the intensity modulation, angle of arrival [9], time of arrival [10], time difference of arrival [14], time of flight (TOF), and direct detection. In VLP systems, linear least square (LLS) or non-linear least square (NLLS) algorithms are often used for the position estimation [15–17].

Despite the fact that the user's mobility can influence the performance of the VLP system, most research reported in the literature has focused primarily on static scenarios. The major issues of shadowing and blocking affecting user's mobility were reported in [18], where the VLC system performance considering the changes in the channel conditions in different indoor scenarios (i.e., a furniture equipped office room, an empty hall, and a corridor) was investigated. It was shown that, the cumulative distribution function (CDF) of the received power distribution differs in the worst case by up to 7% in a furnished office (people density > 0.16 people/m^2). Alternatively, the highest root mean square (RMS) delay spread of 6.5% in comparison with the case with no people was observed for an empty hall. The results also revealed that, the corridor with the maximum RMS delay of 2% at the people density > 0.16 people/m^2 is the most robust against the people's movement compared with the other two where the problem of shadowing or blockage could be readily avoided. Another concern with the user's mobility is the processing time required that needs considering with respect to the speed of movement for the receiver (Rx).

In most of the reported methods, the angular dependency was neglected in RSS-based localization with the assumption that, the Rx has a fixed height and is pointing up towards the Txs [19]. However, computational and implementation costs are too high, and the assumptions made may not be valid in real-time application scenarios with mobile Rxs, which needs further investigation. Recent works have focused on the impact of multipath induced reflections on the performance of VLP without considering the tilting angles [20–22], where it was shown that, multipath reflections considerably increase ε_p; whereas in [23], it was shown that, the channel capacity can be significantly improved by carefully selecting the Rx's tilting angle θ_{Rx}. However, the initial research demonstrated that in VLP θ_{Rx} usually results in increased ε_p (i.e., lower accuracy).

The widely used commercially available LED spotlights in building facilitates the concept of using Txs with tilting features. For instance, the impact of the Tx (LED) tilting angle θ_{Tx} on the accuracy of RSS-based VLP was studied in [24], where it was shown that ε_p increased (i.e., in the order of centimeters) with θ_{Tx}. In [25], a 4-LED VLP system using an artificial neural network (ANN) was proposed to improve the positioning accuracy, which is impacted by the random and unknown static Tx tilt angle with a maximum variation of 2°. It was shown that ANN offered improved performance compared with standard trilateration, achieving localization errors below 1 cm for the line-of-sight (LoS) channel.

In Addition, an RSS-based localization algorithm with multidimensional LED array was proposed in [26], where the design of the lamp structure was introduced to exploit the direction of the LED in a LoS environment. The authors showed that, the proposed system achieved a RMS error of 0.04 and 0.06 m in two- and three-dimensional localization, respectively for the LED with a tilt angle of 15°. While in [27], an angle diversity Tx (ADT) together with accelerometers was proposed for uplink three-dimensional localization in a LoS environment. ADT was a combination of 19 or 37 LEDs (LEDs array), which were placed on the ground, and PDs located on the ceiling. The results showed that, an average localization error of less than 0.15 m.

The impact of non-line of sight (NLoS) path in a VLC system deployed in a referenced empty room has been reported in the literature. In [28], the impact of the power levels from NLoS paths on the performance of VLP for different Rx positions and their orientations was reported. It provided a theoretical framework for the design of VLP resource allocation methods to improve the performance of the non-tilted Tx. Channel modeling and its characterisation with the existence of reflections from objects and surfaces were investigated in [29]. Considering the delay spread and the channel gain in a typical room, it was shown that it is not required to consider all objects within rooms [29,30]. Moreover, the use of flexible organic LED-based VLC in indoor environments (i.e., offices, corridors, semi-open corridors in shopping malls, etc.) was investigated in [31], where it was shown that the channel gain in an empty room is higher by 4.8 and 5.2 dB compared with the fully furnished room and a semi-open corridor, respectively [31].

Unlike previous works, in this paper we investigate LED tilting for the first time and show that it can be beneficial in VLPs in improving the positioning accuracy (PA). We show the impact of reflections on the accuracy by means of the received power from both LoS and NLoS transmission paths, the positioning algorithm utilized, and the accuracy of the VLP system for a single PD-based static Rx (i.e., putting the Rx at fixed locations) where the user movement has not been considered. In this approach, the Txs are oriented towards the pointing center F with the (x_F, y_F, z_F) coordinates without violating the acceptable uniformity range of the light distribution in the illuminated region. Note, F is selected at the center of the receiving plane in this work, and alignment is achieved with respect to the Tx normal $\hat{t}_k$.

We investigate the regression, which is fitted with the received power P_R points at various Rx locations for two different scenarios. Note, the Rx locations are within a squared shape region centered at F with a side length D_r. The polynomial regressions (PRs) are fitted with the PR points for the full and half rooms of areas of 6 × 6 and 3 × 3 m^2, which is termed as scenarios S1 and S2, respectively. The study is carried out using the LLS algorithm for position estimation, which is a low complexity solution. Hence, we offer a significant accuracy improvement by up to ~66% compared with a link without Tx's tilt. We show ε_p of 1.7, and 1.3 cm for S1 and S2, respectively, and for z_F of 0 m (i.e., the height of F from the floor level). Furthermore, we investigate z_F with respect to ε_p and we show that, the lowest ε_p of 1.3 and 0.8 cm were for S1 and S2, respectively.

The remainder of this paper is structured as follows. Section 2 presents the VLC system model used in the positioning algorithm. The positioning algorithm is briefly explained in Section 3. The results and discussion are included in Section 4. Finally, Section 5 provides the conclusion of the paper.

2. Proposed Visible Light Positioning (VLP) System Model

In RSS-based localization systems, positioning accuracy depends mainly on P_R. For NLoS links, reflection from near and far walls should be considered, which contributes to the degradation of PA. For example, Figure 1 illustrates a system with two Txs aligned with respect to F (i.e., shown as the tilted Tx normal $\hat{t}_k$), which is used to investigate the impact of reflections from walls on the accuracy of VLP). Here, the aim is to maximize P_R from the LoS paths to improve accuracy at F, which is initially set at the center of the

receiving plane (i.e., x_F, y_F, and z_F are all set to zero). The tilting orientation is estimated based on the position of F, which is given by:

$$\hat{t}_k = \frac{\vec{T_k}}{\|\vec{T_k}\|}, \tag{1}$$

where $\vec{T_k}$ is a vector that represents the difference between the coordinates of the kth Tx and point F (x_F, y_F, z_F), and $\|\cdot\|$ is the Euclidean norm. The tilted irradiance angle $\omega_{k,w}^{\text{tilt}}$ is given by:

$$\cos\left(\omega_{k,w}^{\text{tilt}}\right) = \frac{d_{k,w} \cdot \hat{t}_k}{\|d_{k,w}\| \cdot \|\hat{t}_k\|}, \tag{2}$$

where $d_{k,w}$ is the distance between the kth Tx and the reflective area, and $\cdot$ represents the product dot operation.

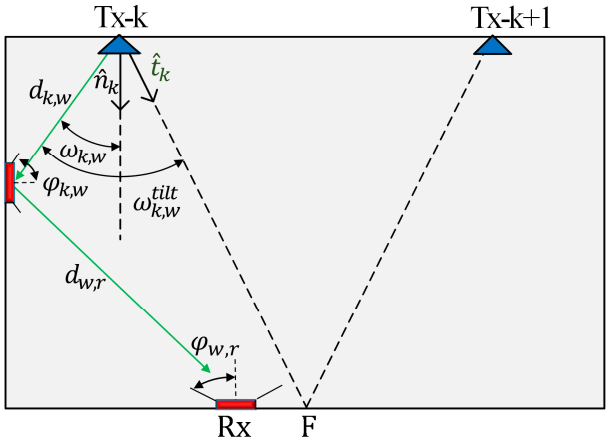

(**a**)

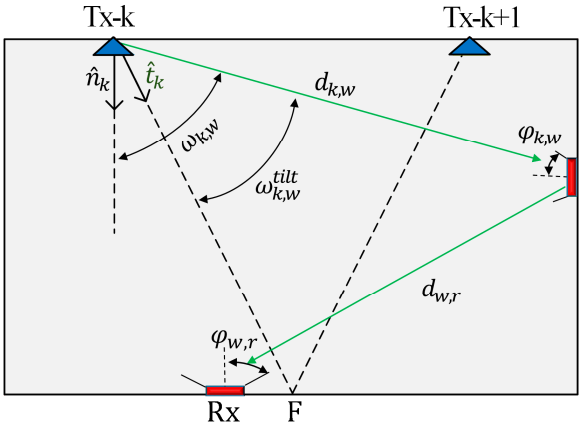

(**b**)

Figure 1. An example of a reflected light ray in case of light-emitting diode (LED) tilt: (**a**) near-wall reflections case, and (**b**) far wall reflections case.

The NLoS power contributions from the near-wall reflections represented by the Tx's cosine terms expressed in (2) can be reduced by tilting the Txs towards F (i.e., $\hat{t}_k$ is directed towards F that implies $\omega_{k,w}^{\text{tilt}} > \omega_{k,w}$, where $\omega_{k,w}$ is the irradiance angle with no tilted Tx, see Figure 1a. Even though the Tx's cosine terms of NLoS signals will increase for the far-wall reflections, which is implied by $\omega_{k,w}^{\text{tilt}} < \omega_{k,w}$, the link experience a higher path

loss due to the longer transmission range, see Figure 1b. Having these observations in mind, we can infer that tilting the Txs can be beneficial in VLP by leveraging the effect of reflections from both near- and far-walls. Under this perspective, it reasonable to explore tilting based on F at the center of the receiving plane and investigate how this can improve PA. These observations remain valid for the entire area of the walls when concerning the first reflection. Higher-order reflections also have an impact on positioning accuracy. However, due to the fact that these higher-order reflections have reduced power levels when compared with the LoS and 1st order case in regions near the center of the room, the previous discussion is still valid, and LoS power can be maximized by tilting towards the center.

Figure 2 shows the geometrical set-up diagram of the proposed indoor VLP system, which is composed of 4 Txs (i.e., LEDs) and an Rx (i.e., a PD) positioned on the ceiling and the floor level, respectively. Each kth Tx has a known set of coordinates (x_k, y_k, z_k), which is associated with the world coordinate system (WCS), with $\hat{t}_k$ of $[\sin\theta_{\mathrm{Tx},k}\cos\alpha_k, \sin\theta_{\mathrm{Tx},k}\sin\alpha_k, -\cos\theta_{\mathrm{Tx},k}]$ where $\theta_{\mathrm{Tx},k}$, α_k are the tilting and azimuth angles, respectively and k is 1, . . . , 4. Note that, in this work, as a reference, an empty room is considered to study the impact of Tx's tilting on the positioning accuracy. The proposed system can be utilized for positioning purposes where the positioning accuracy is a major concern. However, if indoor positioning system uses the already existing wireless communication network architectures, then high accuracy may no longer be critical. Therefore, there exists always a trade-off between accuracy and other system requirements including scalability, complexity, coverage, etc.

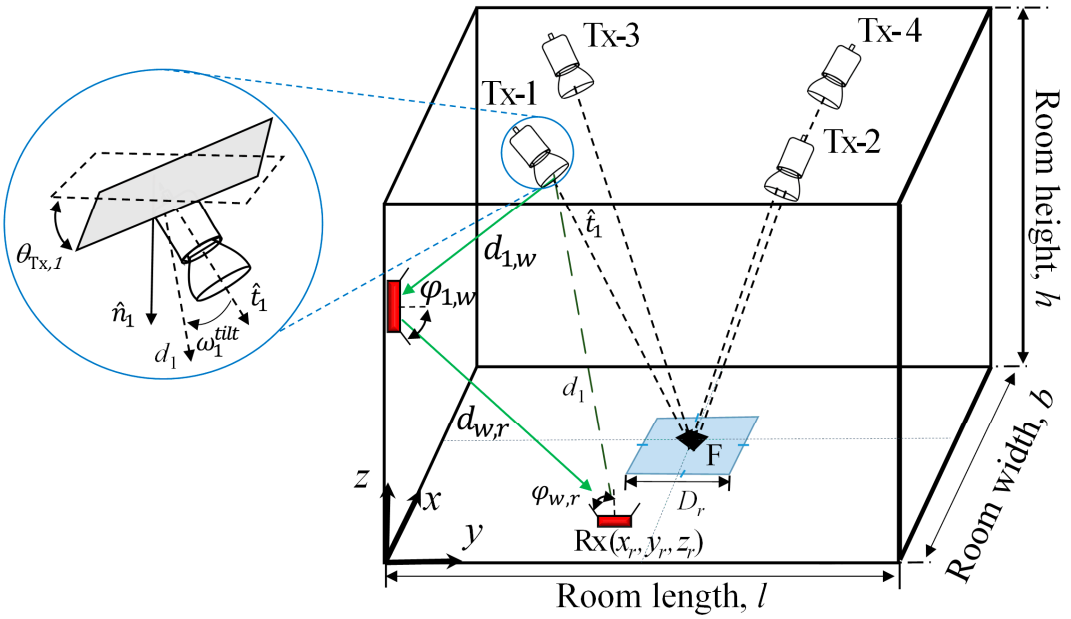

Figure 2. The proposed indoor visible light positioning (VLP) system with the tilted transmitter (Tx).

Each Tx broadcast unique ID information of 2 bits, which is encoded and modulated using on-off keying (OOK), which allows separation at the Rx using a correlation method that can be received at the Rx in advance of location identification, see Figure 3. Considering the 1st order reflections, the received total power is given by:

$$P_R = \sum P_{R-\mathrm{LoS}} + \sum P_{R-\mathrm{NLoS}}, \tag{3}$$

where $P_{R-\mathrm{LoS}}$ and $P_{R-\mathrm{NLoS}}$ represent the received power for LoS and NLoS, respectively. Typically, the signal-to-noise ratio in standard VLC will be high (>20 dB [32]), which would be considered noise-free in common cases). Moreover, noise sources (mostly dominated by the background lights) [32] will have a similar effect on the VLP system with and

without tilting Tx. Thus, a noise-free system is considered in this work. The conventional trilateration technique based on a range of three minimum observation points offers the advantage of simple geometrical solutions [14]. Using the RSS algorithm and 4-Tx (i.e., LEDs), the $P_{R-\mathrm{LoS}}$ for the LoS path is given as [33,34]:

$$\sum P_{R-\mathrm{LoS}} = \sum_{k=1}^{K} C_{\mathrm{o}} P_t \frac{\cos^m\left(\omega_k^{\mathrm{tilt}}\right)\, \cos(\varphi)}{\|d_k\|^2} T_s(\varphi) g(\varphi), \tag{4}$$

where

$$C_{\mathrm{o}} = \frac{m+1}{2\pi} \mathcal{R}\, A_r, \tag{5}$$

and

$$m = -\frac{\ln(2)}{\ln\left(\cos\left(\Theta_{\frac{1}{2}}\right)\right)}, \tag{6}$$

where K is the total number of Txs, $\Theta_{1/2}$ is the light source irradiance half-power angle, ω_k^{tilt} and φ are the tilted irradiance angle from the kth Tx to the Rx and the receiving incident angle, respectively. d_k is the distance between kth Tx and Rx. A_r and $\mathcal{R}$ are the PD's active area and responsivity, respectively. $T_s(\varphi)$ and $g(\varphi)$ are the gains of the optical filter and the concentrator at the Rx, respectively. Note, $T_s\,(\varphi)$ and $g(\varphi)$ are set to unity, $\varphi < 90^\circ$ and $d \gg \sqrt{A_r}$.

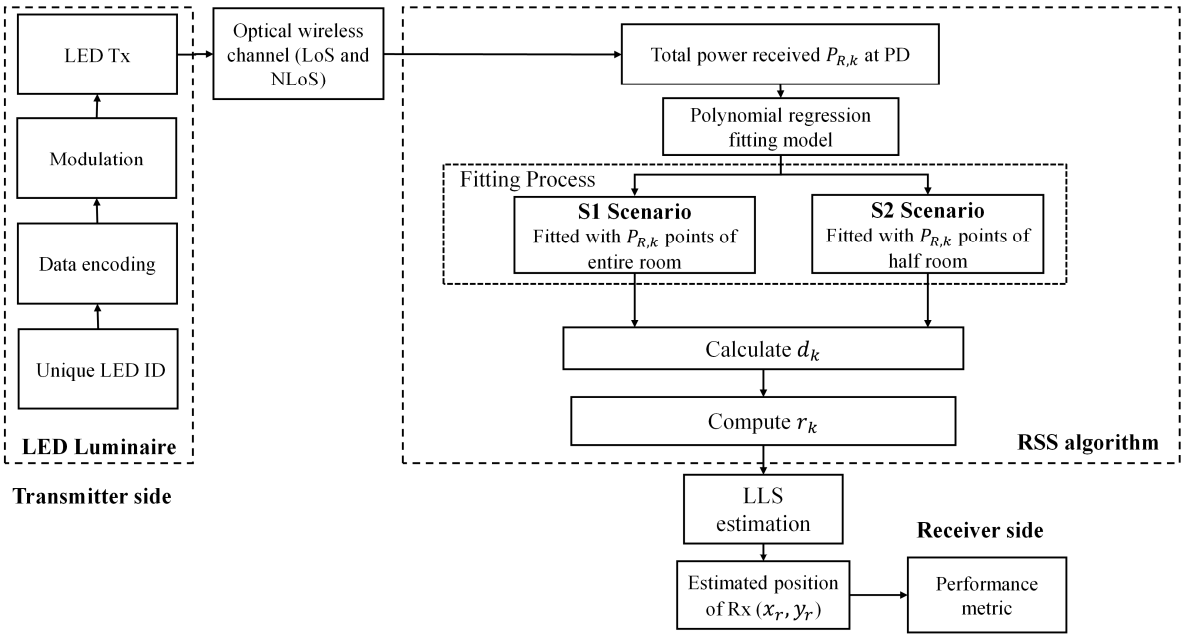

Figure 3. Block diagram of the proposed VLP system.

For the NLoS path and considering only the first-order reflection, the received total power can be expressed as [32]:

$$\sum P_{R-\mathrm{NLoS}} = \sum_{k=1}^{K} \sum_{\mathrm{wall}} \rho C_{\mathrm{o}} P_t A_{\mathrm{ref}} \frac{\cos^m\left(\omega_{k,w}^{\mathrm{tilt}}\right) \cos(\varphi_{k,w})}{\pi(\|d_{k,w}\|\|d_{w,r}\|)^2} T_s(\varphi_{w,r})\, g(\varphi_{w,r}) \cos(\omega_{w,r}) \cos(\varphi_{w,r}), \tag{7}$$

where $d_{k,w}$, $\omega_{k,w}^{\mathrm{tilt}}$, and $\varphi_{k,w}$ are the distances, irradiance angle, and the receiving incident angle between the kth Tx and the reflective area, respectively. $d_{w,r}$, $\omega_{w,r}$, and $\varphi_{w,r}$ are the distances, irradiance angle, and the receiving incident angle between the reflective area and the Rx, respectively, see Figure 1a. ρ is the reflection coefficient, which depends on the material of the reflective surface and A_{ref} is the reflection area. $P_{R-\mathrm{NLoS}}$ for the signals from the NLoS paths is determined based on the Matlab code 3.2 from [32].

Moreover, the uniform distribution of the P_R inside the illuminated zone is essential in indoor environments [16]. The uniformity of light distribution in the room (U) is represented as the ratio of the minimum to maximum power intensity at the receiving plane, which is given by:

$$U = \frac{\min(P_R)}{\max(P_R)}, \tag{8}$$

Here we consider a grid (1 cm resolution) of 3600 Rx positions on the receiving plane, which is associated with WCS of (x_r, y_r, z_r). We have also specified the dedicated region, which is a square shape centered at the point F and located at the receiving plane. The receiving positions are considered inside this region only. All the other key system parameters are given in Table 1.

Table 1. The key system parameters.

Parameter	Symbol	Value
Room size	(l, b, h)	$6 \times 6 \times 3$ m^3
The coordinates of		
Tx-1	(x_1, y_1, z_1)	(−1.7 m, −1.7 m, 3 m)
Tx-2	(x_2, y_2, z_2)	(1.7 m, −1.7 m, 3 m)
Tx-3	(x_3, y_3, z_3)	(−1.7 m, 1.7 m, 3 m)
Tx-4	(x_4, y_4, z_4)	(1.7 m, 1.7 m, 3 m)
Transmit power of each Tx	P_t	1 W
Receiver's field of view	FoV	75°
Reflection coefficient	ρ	0.7
Half power angle	HPA	60°
Photodiode area	A_r	10^{-4} m^2
Responsivity	$\mathcal{R}$	1 A/W
Reflection coefficient	ρ	0.7

3. Positioning Algorithm

3.1. Distance Estimation Using Polynomial Regression

The block diagram of the proposed VLP system is shown in Figure 3, in which P_R is processed to estimate the Rx position. Distance estimation is the central feature of the RSS positioning approach, and for LoS paths it is normally deducted from (4), which is estimated as:

$$\|d_k\|^2 = \|r_k\|^2 + h^2 \tag{9}$$

where h is the vertical distance between the Tx and the Rx. The estimated distance between the Rx and the kth Tx can be estimated from (4), which is given by:

$$r_k = \sqrt{\left(\frac{P_t C_o h^{m+1}}{P_{R-\mathrm{LoS},k}}\right)^{\frac{2}{m+3}} - h^2}, \tag{10}$$

where $P_{R-\mathrm{LoS},\,k}$ is the LoS received power at Rx from kth Tx. In NLoS links, this approach results in increased errors due to reflections [35,36], therefore the distance estimation approach using (10) is no longer valid. One possible approach would be to generate a polynomial fitted model for the power and distance relationship as defined by:

$$d_k = a_0 + a_1 P_{R,k} + a_2 (P_{R,k})^2 + \cdots + a_j (P_{R,k})^j, \tag{11}$$

where a_j is the coefficient of the fitted polynomial at jth degree polynomial and $P_{R,\,k}$ is the total received power at Rx from kth Tx. Note, d_k is computed using (11), which is then substituted into (9) to determine r_k.

3.2. Linear Least Square (LLS) Estimation

LLS is adopted to analyze the performance of the proposed system by considering the estimated distances of the NLoS paths, which is a low complexity solution as compared with the NLLS algorithm. Following geometric properties, a minimum of 3-Tx located at the center of the circle is required, where the estimated distance is considered as the circle radius. The intersection point of the three circles is considered as the measured position of the Rx. E.g., the kth LED luminaire is positioned at (x_k, y_k, z_k) and the Rx is located at (x_r, y_r, z_r). A closed-form solution using the LLS estimation method is given by:

$$X = \left(A^T A\right)^{-1} A^T B \tag{12}$$

where

$$A = \begin{bmatrix} x_2 - x_1 & y_2 - y_1 \\ x_3 - x_1 & y_3 - y_1 \\ x_4 - x_1 & y_4 - y_1 \end{bmatrix}, \quad X = \begin{bmatrix} x_r \\ y_r \end{bmatrix} \tag{13}$$

$$B = 0.5 \times \begin{bmatrix} \left({r_1}^2 - {r_2}^2\right) + \left({x_2}^2 + {y_2}^2\right) - \left({x_1}^2 + {y_1}^2\right) \\ \left({r_1}^2 - {r_3}^2\right) + \left({x_3}^2 + {y_3}^2\right) - \left({x_1}^2 + {y_1}^2\right) \\ \left({r_1}^2 - {r_4}^2\right) + \left({x_4}^2 + {y_4}^2\right) - \left({x_1}^2 + {y_1}^2\right) \end{bmatrix}. \tag{14}$$

4. Results and Discussion

4.1. Impact of the Transmitter (Tx) Tilting on the Radiation Pattern

Figure 4a shows the received power distributions for the link (i.e., received signal strength indicator RSSI) with and without the tilting Txs. Note, the Txs are directed towards F following the proposed model in Section 2. As shown in Figure 4b, there is a significant improvement in the power distribution with the tilting Txs (i.e., a much more uniform distribution) around the center of the receiving plane. All the observed tilted Tx normal $\hat{t}_k$ for 4-Tx are given in Table 2.

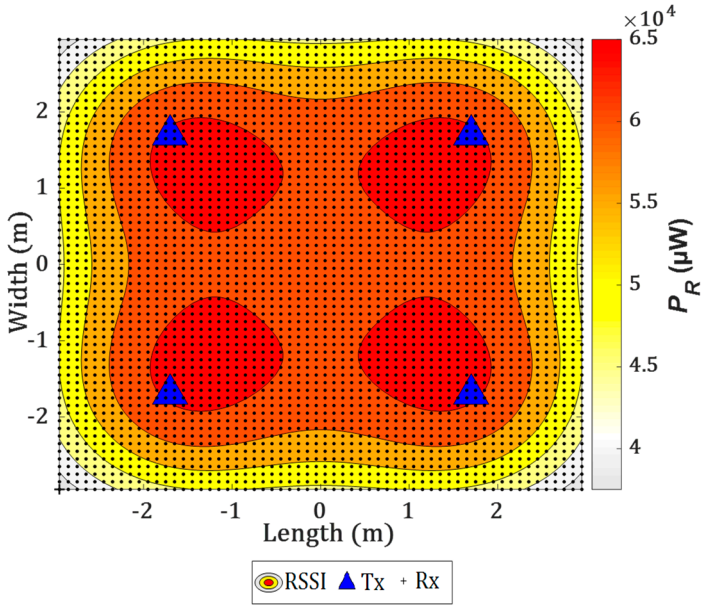

(**a**)

Figure 4. *Cont.*

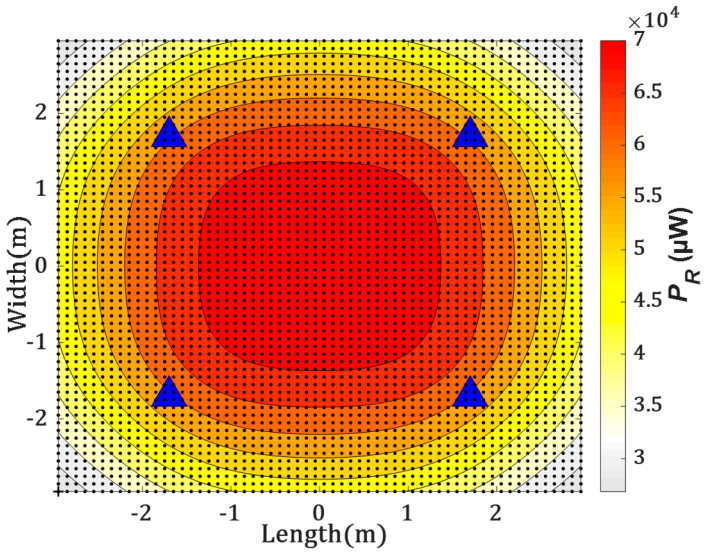

(**b**)

Figure 4. The received power distributions for the proposed system for the Txs with: (**a**) no tilting, and (**b**) tilting.

Table 2. The values of tilted Tx normal for all Txs.

Tx Number	Tilted LED Normal, $\hat{t}_k$
Tx-1	[0.4, 0.4, −0.8]
Tx-2	[−0.4, 0.4, −0.8]
Tx-3	[0.4, −0.4, −0.8]
Tx-4	[−0.4, −0.4, −0.8]

4.2. Polynomial Fitting

With reference to Figure 3, d_k is estimated based on $P_{R,k}$ and the PR (polynomial regression) method as outlined in Section 3.1. The accuracy and precision of fitting are measured by the coefficient of determination R^2, which is a statistical measure of how close the data are to the fitted regression line, and the standard deviation. Note, PR is considered for various data points and categorized into two scenarios S1 and S2 based on the room dimensions. For scenarios S1 and S2, the PRs are fitted with the $P_{R,k}$ points for the full and half rooms of areas of 6×6 and 3×3 m^2, respectively. The deviation of $P_{R,k}$ points is impacted mainly by the reflections wherein the data near the walls imply a larger estimation error as stated previously in the literature [19,32]. Therefore, 3600 samples (a full room with a 1 cm grid size) are considered for the polynomial fitting for S1, while for S2 we only have considered 900 samples (an inner half room). A stabilized residual sum of squares is achieved with the polynomial order j of 4. The polynomial coefficients of the fitted curve and R^2 are estimated for both S1 and S2.

The polynomial fitted curves for VLP without and with the tilting Txs are illustrated in Figure 5. The green points and blue plots indicate the $P_{R,k}$ points for the full and half rooms, respectively. Figure 5a shows that, the $P_{R,k}$ points span between 0 and 4.2 mW, and are uniformly distributed for both S1 and S2. However, Figure 5b depicts that the $P_{R,k}$ points for S1 are more scattered with a smaller span of 0.5 to 3.2 mW, which corresponds to the corner of the room. In S2, the $P_{R,k}$ points are more focused towards S2 due to tilting of the Tx, thus the fitting data points are considered for S2 only. From the results obtained, both R^2 and the standard deviation are positively affected with tilting of the Tx, i.e., higher R^2 value of 0.98 and lower standard deviation of 0.98 is achieved for the tilted Tx as compared with a lower R^2 value of 0.96 and higher standard deviation of 1.01 in the case of no tilted

Tx, see Figure 5b. Table 3 shows the estimated polynomial coefficients and R^2 values for S2 with and without the tilted Txs.

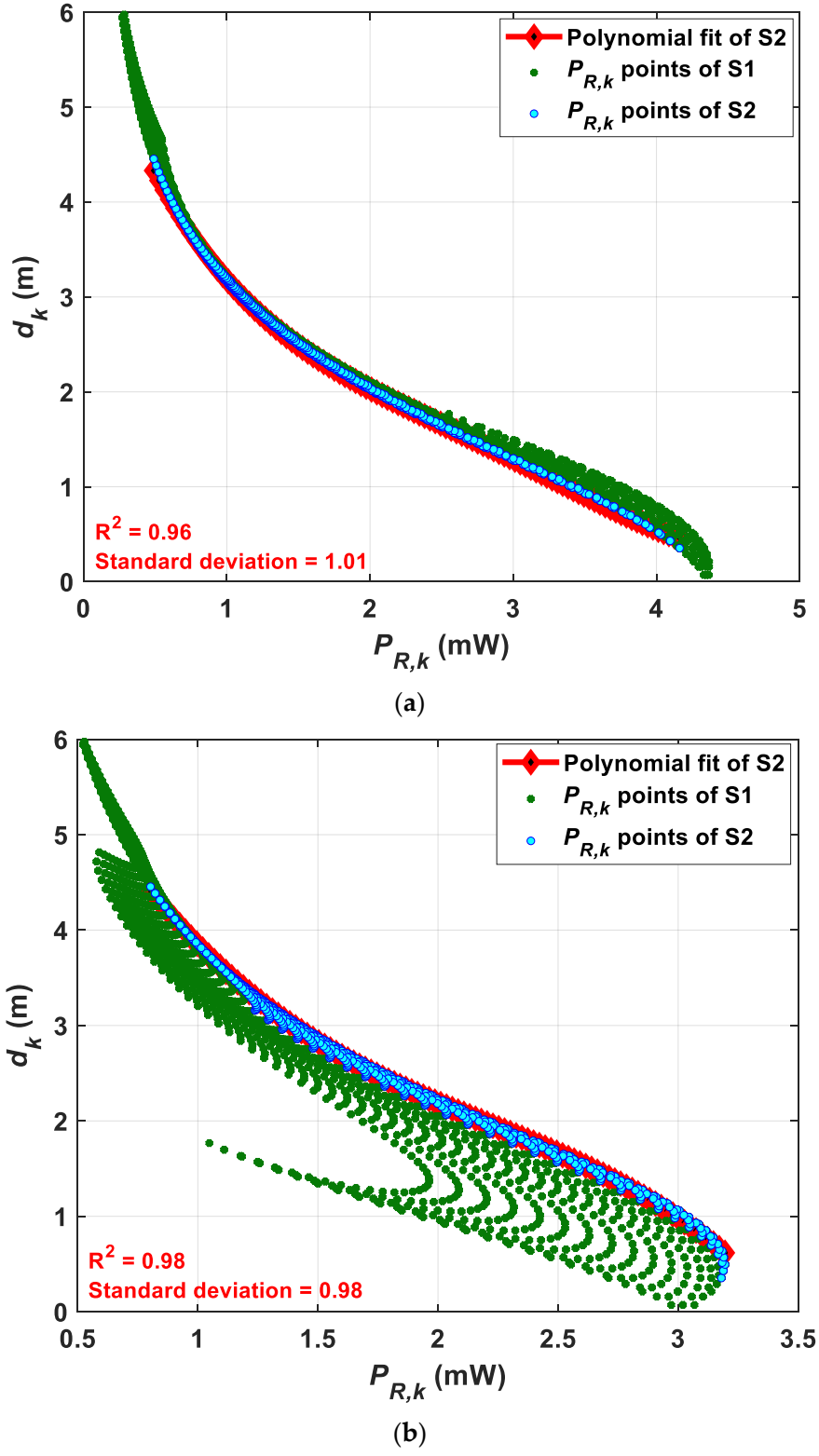

Figure 5. The distance estimation for Tx-k using the polynomial regression (PR) method employed in S2 for the Txs with: (**a**) no tilting, and (**b**) tilting.

Table 3. The coefficients of the polynomial fitted curve for the scenario S2.

Cases	Estimated Polynomial Coefficients (No Units)					R^2
	a_0	a_1	a_2	a_3	a_4	
With tilted Tx	7.38×10^4	-3.60×10^5	2.37×10^4	-6.26×10^2	8.10	0.98
Without tilted Tx	8.86×10^6	9.93×10^5	3.96×10^4	7.35×10^2	7.44	0.96

4.3. Impact of the Tx Tilting and the Altitude of F on VLP

In this section, we investigate ε_p for different values of D_r to realize the impact of tilted Txs near the center of the receiving plane, and further analyze the impact of changing the height of z_F on the positioning accuracy. Figure 6 illustrates Inv(90%) as a function of D_r for S1 and S2 with the LLS algorithm, which is applied for the case with LoS and NLoS paths to estimate the Rx's position, as described in Section 3. The quantile function Inv(χ) is used as a performance metric to observe the confidence interval of ε_p, which is given by:

$$\varepsilon_{p,\chi} = \text{Inv}(\chi) = \text{CDF}^{-1}(\chi) \tag{15}$$

where χ is the percentage of the confidence interval, and CDF represents the cumulative distribution function of ε_p.

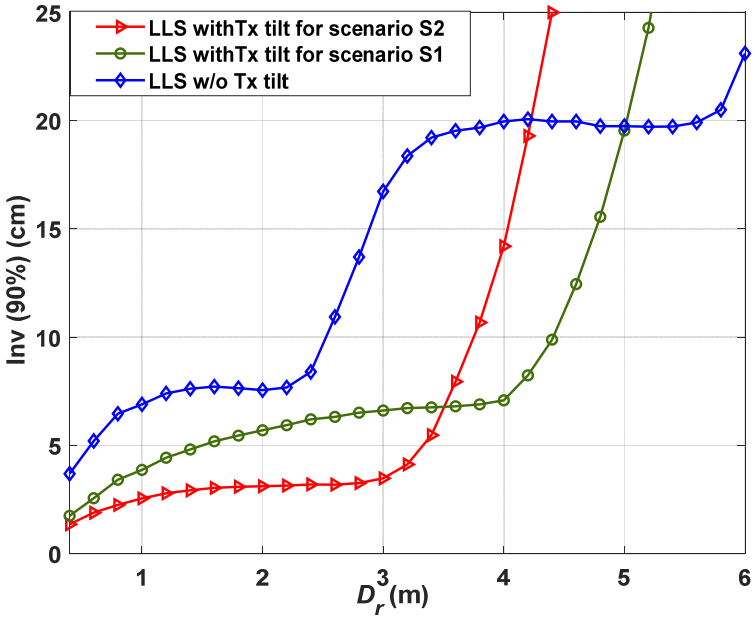

Figure 6. The measured quantile function at χ of 90% for various D_r for linear least square (LLS) with and without the tilted Txs.

To ensure a VLP link with high reliability, we have selected a 90% confidence interval for ε_p to include the majority of the measured points. Note that, the Txs' tilting angle is fixed at the point F for all values of D_r. Moreover, the error can be reduced significantly depending on S1 or S2. For instance, for S1, ε_p values of 1.7 and 3.6 cm are obtained for both tilting and non-tilting scenarios, respectively for D_r of 40 cm. In addition, we have achieved the accuracy improvement of 44, 24, 60, and 64% for D_r of 1, 2, 3, and 4 m, respectively with the maximum accuracy improvement of 66% for D_r of 3.6 m. In addition, for S2, ε_p of 1.3 cm is obtained for the observation area with D_r of 40 cm with the tilted Tx. Hence, the Tx's tilting (LED tilting angle) can improve the positioning accuracy in both S1 and S2 with the same detection area of 5×5 m^2 (up to D_r of 5 m) as compared with the case with non-tilting Tx. This could be explained by the fact that, for large observation areas (i.e., large D_r), the CDF of the error becomes affected by the walls and corners of the

room, with no improvement in the accuracy. Hence, the NLoS paths become dominant for regions far away from the point F, which degrades the positioning accuracy. Therefore, the proposed VLP system with the tilted Txs outperforms the system with no tilting Txs for almost the entire room i.e., an area of 5×5 m^2.

We further analyze the impact of changing the height of pointing center F (i.e., z_F) on the positioning accuracy, which is eventually the variation in the Tx's tilting. Figure 7 depict the Inv(90%) as a function of D_r for a range z_F (i.e., -2 to 2 m) with and without the tilting Txs for S1 and S2. Note that, a high negative value of z_F implies that the Tx is pointing vertically downwards towards the Rx. For instance, $-\infty$ for z_F corresponds to the standard non-tilted case and it does not imply reception under the floor. From the Figure 7, it is observed that, (i) ε_p increases and decreases s with the positive and negative values of z_F (i.e., $z_F > 0, < 0$), respectively for both S1 and S2; (ii) the minimum ε_p of 1.3 cm is at z_F of -0.5 m compared with 1.7 cm for z_F of 0 m for S1 with D_r of 40 cm, see Figure 7a; and (iii) the lowest ε_p is achieved at $-2 < z_F < 0$ m depending on the value of D_r. The proposed VLP system can be further improved for the regions with D_r of up to 5.5 m by adjusting the negative value of z_F. For S2, the minimum ε_p of 0.8 cm is observed at z_F of -2 m and D_r of 40 cm compared with 1.3 cm at F (i.e., $z_F = 0$ m), see Figure 7b. However, the case with tilting Txs offers the lowest ε_p for D_r up to 4.36 m.

Finally, Figure 8 shows the uniformity of light distribution U against D_r without and with the tilting Tx and a range of z_F. The dashed line represents the EN 12464-1 European standard of lighting in an indoor environment [37], which defines the minimum acceptable ranges of uniformity of the light distribution. We have shown that the proposed VLP system with the tilting Txs is capable of providing higher uniformity for the entire room for $z_F \leq -1$ m. The uniformity of the VLP system with tilted Tx increases with the decreased value of z_F.

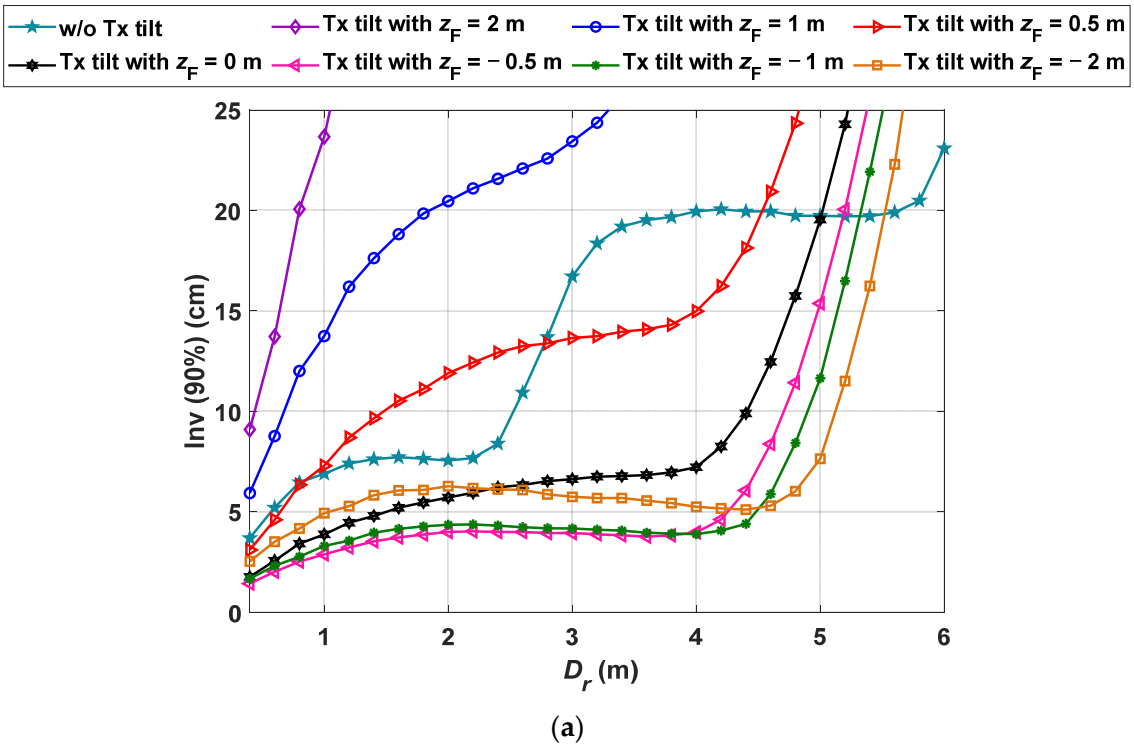

(a)

Figure 7. *Cont.*

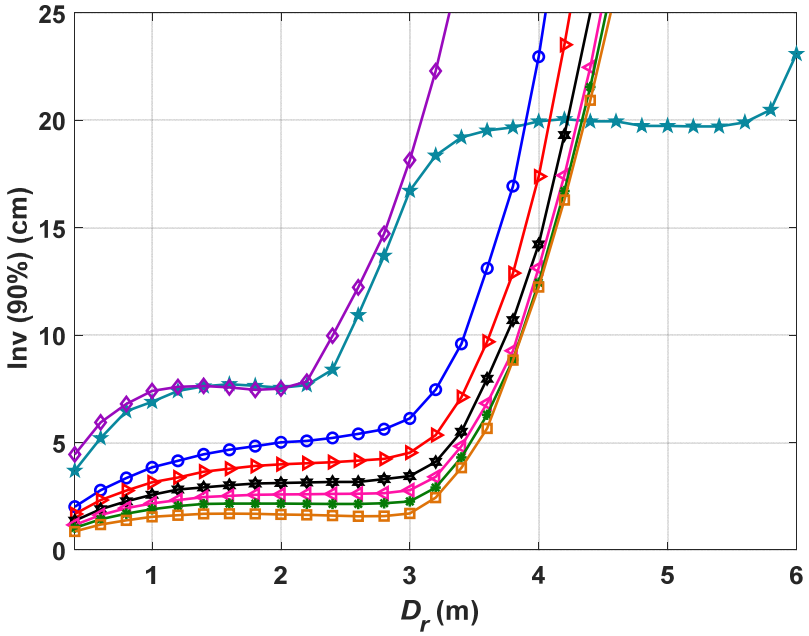

(**b**)

Figure 7. The measured quantile function at χ of 90% for various z_F values for: (**a**) S1, and (**b**) S2.

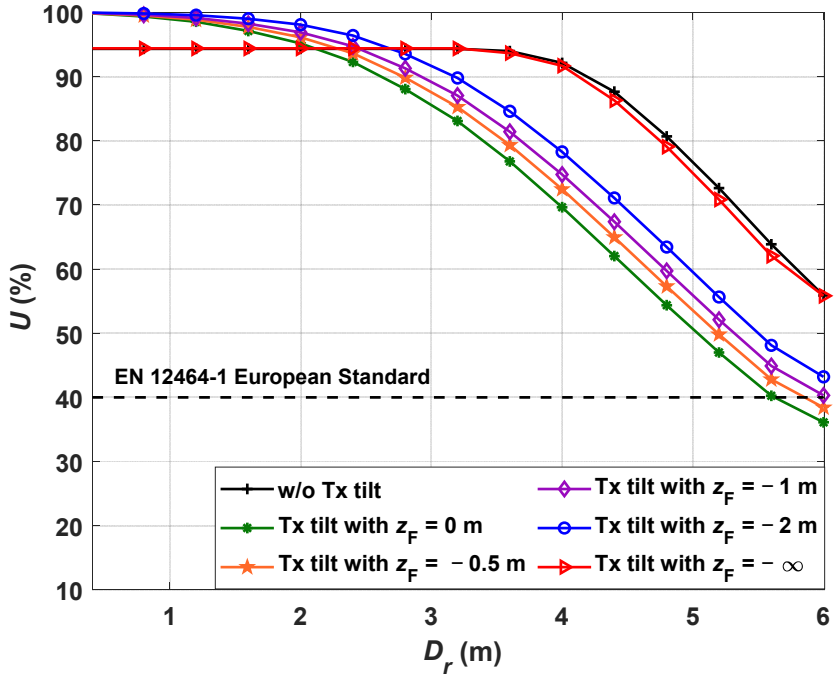

Figure 8. The uniformity of light distribution in different D_r *w/o* and with the tilting Txs.

5. Conclusions

In this paper, a novel approach was proposed to achieve a highly accurate indoor VLP system by considering multipath reflections. Initially, the Tx was tilted towards the center of the receiving plane to achieve higher accuracy by maximizing the received power level due to contributions from the LoS paths at the pointing center F. The positioning error was estimated by using the LLS algorithm with polynomial regression. We investigated the regression fitted with the received power points for two scenarios of S1 and S2. The results

showed a significant improvement in the accuracy by up to ~66% compared with a typical non-tilting Tx case. In addition, positioning errors of 1.7, and 1.3 were obtained for the tilted Tx for S1 and S2, respectively at z_F of 0 m. The results also showed that, the uniformity of the proposed VLP system in line with European Standard EN 12464-1, therefore meeting the uniformity requirement of the visible illumination regions. Furthermore, we improved the accuracy of the proposed VLP system by controlling the height of F by achieving the lowest ε_p of 1.3 and 0.8 cm for S1 and S2, respectively. Ultimately, it was concluded that the proposed VLP system with the tilting Tx outperforms the non-tilted Tx scenario. Likewise, we could gain lower ε_p when considering S2, whereas ε_p will increase with D_r as indicated for S1.

Author Contributions: The contributions of the authors in this paper are the following: conceptualization: N.C., O.I.Y., L.N.A., and Z.G.; investigation: N.C., and O.I.Y.; methodology: N.C., O.I.Y., L.N.A. and Z.G.; project administration: L.N.A., Z.G., and S.Z.; software: N.C., and O.I.Y.; validation: L.N.A., Z.G., S.Z., and H.L.-M. All authors have read and agreed to the published version of the manuscript.

Funding: This research was funded by H2020/MSCA-ITN funding program under the framework of the European Training Network on Visible Light Based Interoperability and Networking, project (VisIoN) grant agreement No 764461. One of the authors (Othman Isam Younus) is funded by the Northumbria University Ph.D. scholarship.

Institutional Review Board Statement: Not applicable.

Informed Consent Statement: Not applicable.

Conflicts of Interest: The authors declare no conflict of interest.

Abbreviations

Short Form	Description
ADT	Angle diversity transmitter
ANN	Artificial neural network
CDF	Cumulative distribution function
IS	Image sensor
LEDs	Light-emitting diodes
LLS	Linear least square
LoS	Line of sight
NLLS	Nonlinear least square
NLoS	Non-line of sight
OOK	On-off keying
PA	Positioning accuracy
PDs	Photodiodes
PR	Polynomial regression
RF	Radio frequency
RMS	Root mean square
RSS	Received signal strength
RSSI	Received signal strength indicator
Rx	Receiver
TOF	Time of flight
Tx	Transmitter
VLC	Visible light communication
VLP	Visible light positioning
WCS	World coordinate system

References

1. Nguyen, C.T.; Saputra, Y.M.; Huynh, N.V.; Nguyen, N.-T.; Khoa, T.V.; Tuan, B.M.; Nguyen, D.N.; Hoang, D.T.; Vu, T.X.; Dutkiewicz, E.; et al. A Comprehensive Survey of Enabling and Emerging Technologies for Social Distancing—Part I: Fundamentals and Enabling Technologies. *IEEE Access* **2020**, *8*, 153479–153507. [CrossRef]
2. Luo, J.; Fan, L.; Li, H. Indoor Positioning Systems Based on Visible Light Communication: State of the Art. *IEEE Commun. Surv. Tutor.* **2017**, *19*, 2871–2893. [CrossRef]
3. Armstrong, J.; Sekercioglu, Y.A.; Neild, A. Visible Light Positioning: A Roadmap for International Standardization. *IEEE Commun. Mag.* **2013**, *51*, 68–73. [CrossRef]
4. Chung, J.; Donahoe, M.; Schmandt, C.; Kim, I.-J.; Razavai, P.; Wiseman, M. Indoor location sensing using geo-magnetism. In Proceedings of the 9th International Conference on Mobile Systems, Applications, and Services, Washington, DC, USA, 29 June–1 July 2011; pp. 141–154.
5. Youssef, M.; Agrawala, A. The Horus WLAN location determination system. In Proceedings of the 3rd International Conference on Mobile Systems, Applications, and Services, Washington, DC, USA, 6–8 June 2005; pp. 205–218.
6. Chen, Y.; Lymberopoulos, D.; Liu, J.; Priyantha, B. FM-based indoor localization. In Proceedings of the 10th International Conference on Mobile Systems, Applications, and Services, Low Wood Bay, Lake District, UK, 26–28 June 2012; pp. 169–182.
7. Elgala, H.; Mesleh, R.; Haas, H. Indoor optical wireless communication: Potential and state-of-the-art. *IEEE Commun. Mag.* **2011**, *49*, 56–62. [CrossRef]
8. Maheepala, M.; Kouzani, A.Z.; Joordens, M.A. Light-Based Indoor Positioning Systems: A Review. *IEEE Sens. J.* **2020**, *20*, 3971–3995. [CrossRef]
9. Do, T.H.; Yoo, M. An in-Depth Survey of Visible Light Communication Based Positioning Systems. (in eng). *Sensors* **2016**, *16*, 678. [CrossRef]
10. Chaudhary, N.; Alves, L.N.; Ghassemlooy, Z. Current Trends on Visible Light Positioning Techniques. In Proceedings of the 2019 2nd West Asian Colloquium on Optical Wireless Communications (WACOWC), Teheran, Iran, 27–28 April 2019; pp. 100–105.
11. Lee, J.; Kim, S.; Han, S. 3D Visible Light Indoor Positioning by Bokeh Based Optical Intensity Measurement in Smartphone Camera. *IEEE Access* **2019**, *7*, 91399–91406. [CrossRef]
12. Cheng, H.; Xiao, C.; Ji, Y.; Ni, J.; Wang, T. A Single LED Visible Light Positioning System Based on Geometric Features and CMOS Camera. *IEEE Photonics Technol. Lett.* **2020**, *32*, 1097–1100. [CrossRef]
13. Younus, O.I.; Hassan, N.B.; Ghassemlooy, Z.; Haigh, P.A.; Zvanovec, S.; Alves, L.N.; Minh, H.L. Data Rate Enhancement in Optical Camera Communications Using an Artificial Neural Network Equaliser. *IEEE Access* **2020**, *8*, 42656–42665. [CrossRef]
14. Rabadan, J.; Guerra, V.; Guerra, C.; Rufo, J.; Perez-Jimenez, R. A Novel Ranging Technique Based on Optical Camera Communications and Time Difference of Arrival. *Appl. Sci.* **2019**, *9*, 2382. [CrossRef]
15. Zhuang, Y.; Hua, L.; Qi, L.; Yang, J.; Cao, P.; Cao, Y.; Wu, Y.; Thompson, J.; Haas, H. A Survey of Positioning Systems Using Visible LED Lights. *IEEE Commun. Surv. Tutor.* **2018**, *20*, 1963–1988. [CrossRef]
16. Chaudhary, N.; Alves, L.N.; Ghassemlooy, Z. Impact of Transmitter Positioning Uncertainty on RSS-based Visible Light Positioning Accuracy. In Proceedings of the 12th International Symposium on Communication Systems, Networks & Digital Signal Processing (CSNDSP), Porto, Portugal, 20–22 July 2020.
17. Plets, D.; Almadani, Y.; Bastiaens, S.; Ijaz, M.; Martens, L.; Joseph, W. Efficient 3D trilateration algorithm for visible light positioning. *J. Opt.* **2019**, *21*, 05LT01. [CrossRef]
18. Chvojka, P.; Zvanovec, S.; Haigh, P.A.; Ghassemlooy, Z. Channel Characteristics of Visible Light Communications within Dynamic Indoor Environment. *J. Lightwave Technol.* **2015**, *33*, 1719–1725. [CrossRef]
19. Naz, A.; Asif, H.M.; Umer, T.; Ayub, S.; Al-Turjman, F. Trilateration-based indoor localization engineering technique for visible light communication system. *Softw. Pract. Exp.* **2020**, 1–14.
20. Gu, W.; Aminikashani, M.; Deng, P.; Kavehrad, M. Impact of Multipath Reflections on the Performance of Indoor Visible Light Positioning Systems. *J. Lightwave Technol.* **2016**, *34*, 2578–2587. [CrossRef]
21. Plets, D.; Eryildirim, A.; Bastiaens, S.; Stevens, N.; Martens, L.; Joseph, W. A Performance Comparison of Different Cost Functions for RSS-Based Visible Light Positioning Under the Presence of Reflections. In Proceedings of the 4th ACM Workshop on Visible Light Communication Systems, Snowbird, UT, USA, 16 October 2017.
22. Liu, Y.; Zhang, J.; Liu, Y.; Chen, B.; Liu, S.; Zuo, Y. A new indoor visible light positioning scheme to reduce the influence of reflections. In Proceedings of the 17th International Conference on Optical Communications and Networks (ICOCN2018), Zhuhai, China, 16–19 November 2018.
23. Wang, J.-Y.; Li, Q.-L.; Zhu, J.-X.; Wang, Y. Impact of receiver's tilted angle on channel capacity in VLCs. *Electron. Lett.* **2017**, *53*, 421–423. [CrossRef]
24. Plets, D.; Bastiaens, S.; Martens, L.; Joseph, W. An Analysis of the Impact of LED Tilt on Visible Light Positioning Accuracy. *Electronics* **2019**, *8*, 389. [CrossRef]
25. Raes, W.; Stevens, N. Performance Assessment of Artificial Neural Networks on the RSS-Based Visible Light Positioning Accuracy with Random Transmitter Tilt. In Proceedings of the International Symposium on Communication Systems, Networks and Digital Signal Processing (CSNDSP), Porto, Portugal, 20–22 July 2020.

26. Lixuan, W.; Caili, G.; Luo, P.; Li, Q. Indoor visible light localization algorithm based on received signal strength ratio with multi-directional LED array. In Proceedings of the 2017 IEEE International Conference on Communications Workshops (ICC Workshops), Paris, France, 21–25 May 2017; pp. 138–143.
27. Yin, L.; Wu, X.; Haas, H. Indoor Visible Light Positioning with Angle Diversity Transmitter. In Proceedings of the 2015 IEEE 82nd Vehicular Technology Conference (VTC2015-Fall), Boston, MA, USA, 6–9 September 2015; pp. 1–5.
28. Zhou, B.; Liu, A.; Lau, V. Performance Limits of Visible Light-Based User Position and Orientation Estimation Using Received Signal Strength Under NLOS Propagation. *IEEE Trans. Wirel. Commun.* **2019**, *18*, 5227–5241. [CrossRef]
29. Miramirkhani, F.; Uysal, M. Channel Modeling and Characterization for Visible Light Communications. *IEEE Photonics. J.* **2015**, *7*, 1–16. [CrossRef]
30. Uysal, M.; Miramirkhani, F.; Narmanlioglu, O.; Baykas, T.; Panayirci, E. IEEE 802.15.7r1 Reference Channel Models for Visible Light Communications. *IEEE Commun. Mag.* **2017**, *55*, 212–217. [CrossRef]
31. Chaleshtori, Z.N.; Ghassemlooy, Z.; Eldeeb, H.B.; Uysal, M.; Zvanovec, S. Utilization of an OLED-Based VLC System in Office, Corridor, and Semi-Open Corridor Environments. *Sensors* **2020**, *20*, 6869. [CrossRef] [PubMed]
32. Ghassemlooy, Z.; Popoola, W.; Rajbhandari, S. *Optical Wireless Communications: System and Channel Modelling with Matlab®*, 2nd ed.; CRC Press: Boca Raton, FL, USA, 2019.
33. Chaudhary, N.; Alves, L.N.; Ghassemblooy, Z. Feasibility Study of Reverse Trilateration Strategy with a Single Tx for VLP. In Proceedings of the 2019 2nd West Asian Colloquium on Optical Wireless Communications (WACOWC), Teheran, Iran, 27–28 April 2019; pp. 121–126.
34. Younus, O.I.; Minh, H.L.; Dat, P.T.; Yamamoto, N.; Pham, A.T.; Ghassemlooy, Z. Dynamic Physical-Layer Secured Link in a Mobile MIMO VLC System. *IEEE Photonics J.* **2020**, *12*, 1–14. [CrossRef]
35. Shawky, S.; El-Shimy, M.A.; El-Sahn, Z.A.; Rizk, M.R.M.; Aly, M.H. Improved VLC-based indoor positioning system using a regression approach with conventional RSS techniques. In Proceedings of the 2017 13th International Wireless Communications and Mobile Computing Conference (IWCMC), Valencia, Spain, 26–30 June 2017; pp. 904–909.
36. Sun, X.; Duan, J.; Zou, Y.; Shi, A. Impact of multipath effects on theoretical accuracy of TOA-based indoor VLC positioning system. *Photonics Res.* **2015**, *3*, 296–299. [CrossRef]
37. De Normalisation, C.E. *EN 12464-1: Light and Lighting-Lighting of Work Places, Part 1: Indoor Work Places*; BSI: London, UK, 2002.